Scalable Computing: Practice and Experience, ISSN 1895-1767, http://www.scpe.org
© 2025 SCPE. Volume 26, Issues 3, pp. 1429–1439, DOI 10.12694/scpe.v26i3.4167

# BUILDING ENERGY SYSTEMS USING DIGITAL TWINS AND GENETIC ALGORITHMS

JIFENG HAN* AND LIQIN AI†

**Abstract.** In order to solve the problems of energy consumption behavior and production process generating heat waste and carbon emissions, the author proposes to use digital twins and genetic algorithms to study building energy systems. The author employed Matlab/Simulink to develop an optimization framework for isolated multi-energy complementary building energy systems. The optimization objective was to minimize the annual cost of the system, and based on digital twins and genetic algorithms, the model was optimized and simulated for analysis. The experimental results show that compared to not considering flexible loads, when flexible electrical loads, flexible thermal loads, and flexible electrical/thermal loads participate in regulation, the annual cost of the system is reduced by 5.13%, 33.01%, and 35.4%, respectively. Incorporating flexible electrical loads into regulation shifts energy demand towards periods of high photovoltaic output, thereby reducing the required capacities of energy storage batteries and diesel generators. Compared to scenarios where only flexible thermal loads participate in regulation, simultaneous participation of both flexible electrical and thermal loads results in smoother indoor temperature fluctuations with reduced amplitude. When flexible thermal and electrical loads are simultaneously regulated, the best effect is achieved in reducing the annual value of system costs and annual carbon dioxide emissions.

**Key words:** Multi energy complementarity, Flexible load, Digital twin, Isolated building energy systems, genetic algorithm

**1. Introduction.** As national society progresses, industrialization advances, and living standards rise, the demand for energy continues to grow steadily [1]. The total energy consumption of building energy systems is high and is influenced by weather, indoor personnel behavior, and comfort needs. It mainly consumes a large proportion of energy in cooling, heating, and lighting systems. Therefore, the optimization of building energy system operation and energy-saving strategies have received widespread attention from scholars [2].

The traditional energy consumption method usually uses manual methods to predict resources and optimize scheduling in real-time based on the predicted resources; This method has the disadvantages of many uncertain factors, a small range of scheduling strategy selection, and large prediction errors [3]. For example, due to information asymmetry among users, between users and the power grid, or between users, energy conservation and emission reduction goals cannot be achieved, and the requirements for equipment performance among users are inconsistent or even deviate from the goals; It is difficult to achieve when resources are optimized and scheduling strategies are configured to achieve this goal; The energy consumption behavior and production process generate problems such as heat waste and carbon emissions that are difficult to eliminate [4]. Therefore, in order to further achieve the goal of efficient energy conservation and emission reduction, it is necessary to conduct unified analysis and optimization of various resources, and dynamically analyze and simulate them to obtain scheduling strategies with universal laws and good targeting and energy-saving effects. By using digital twin and genetic algorithm technology, a dynamic energy efficiency model is constructed and applied to the overall planning of the comprehensive energy platform to achieve goals such as improving energy utilization efficiency and reducing energy consumption. Establishing a multi energy complementary building energy system that couples renewable energy and traditional energy can effectively overcome the intermittency and volatility of renewable energy, which is of great significance for ensuring the reliability and stability of energy supply in isolated rural areas and achieving local energy self-sufficiency [5,6].

**2. Literature Review.** Due to the intermittent and fluctuating characteristics of renewable energy, it is difficult to match the supply and demand of multi energy complementary building energy systems. The integration of energy storage devices is an important technology for achieving supply-demand balance in re-

*Nanchang Institute of Science & Technology, Nanchang, 330108, China.
†Nanchang Institute of Science & Technology, Nanchang, 330108, China.(Corresponding author, aili118899@163.com)

newable energy systems at present, but relying solely on energy storage devices for regulation will greatly increase system costs [7-8]. Flexible load regulation refers to a type of method that optimizes the load curve by actively changing the load operating time or load size, and has become a hot research topic for domestic and foreign industry scholars due to its economic and efficient characteristics [9]. Libralato, M. et al. created a digital twin to analyze the energy consumption of building HVAC systems. They detailed the programming and data analysis framework of the supervisory system. The digital twin was then employed to compare two control strategies for summer thermostat regulation, aiming to enhance the energy efficiency of building HVAC systems and leverage the thermal storage properties of building envelope structures to modify and reduce peak power demand [10]. Ohmura, T. et al. presented a use case examining optimal scheduling and energy-saving parameters. The study revealed that certain parameter configurations could reduce work waiting time by up to 70% and decrease energy consumption by 1.2% during peak system activity. Consequently, this digital twin demonstrated the feasibility for system administrators to accurately adjust various parameters without disrupting system operations [11]. Hou, Y. et al. introduced a combined simulation framework for energy auditing and pixel-level simulation of building envelope structures that integrates with Digital Twins (DT). This framework initially examines the input and output interactions between the Building Physics Twin (PT) and DT for energy auditing, highlighting the current technical challenges in transferring data from PT to DT for building energy simulation. Additionally, it evaluates the requirements for building parameters in simulations and identifies the existing research gap in model updates between Building Information Modeling (BIM) and Building Energy Modeling (BEM). Furthermore, the framework presents joint simulation methods for building energy simulation, detailing how to exchange data within the joint simulation and interpret the results to develop renovation plans [12].

The above research comprehensively analyzed the impact of digital twins and genetic algorithms on the capacity configuration of energy system equipment, but the research objects are mostly limited to multi input single output microgrid systems. The author aims to establish a matching mechanism between multi type heterogeneous energy combination supply and flexible demand, establish an isolated multi energy complementary building energy system design optimization model for solving multi input and multi output, and analyze and summarize the effect of flexible electricity/heat load on the overall performance of the system through specific cases. The research results can lay a theoretical foundation for the planning and design of distributed multi energy complementary building energy systems in villages.

## 3. Method.

**3.1. Principle of Thermal Power Supply.** The isolated multi energy complementary building energy system consists of photovoltaic modules, solar collectors, air source heat pumps, diesel generators, energy storage batteries, and heat storage water tanks (see Figure 1). The system can be divided into two major components: Power supply system and heating system. In the power supply system, photovoltaic modules serve as the main power supply equipment, and diesel generators serve as auxiliary power supply equipment to supply power to air source heat pumps, electric heaters, and buildings [13,14]; In the heating system, solar collectors serve as the main heating equipment, while air source heat pumps and electric heaters serve as auxiliary heating equipment to provide heat to buildings. The energy storage equipment of the system consists of a heat storage water tank and energy storage batteries.

**3.2. Heating control strategy.** The operation of a solar collector is influenced by the temperature difference between its inlet and outlet, as well as the maximum temperature of the heat storage tank. Similarly, the start and stop of an air source heat pump and electric heater are affected by the upper temperature limit of the heat storage tank. The heating control strategy is illustrated in Figure 3.2. In this figure, the upper temperature limit of the heat storage tank is set at $50°C$. The temperature differences for starting and stopping the solar collector are $5°C$ and $2°C$, respectively. For the air source heat pump, the start and stop temperatures are $40°C$ and $45°C$, while the start temperature for the electric heater is $40°C$.

**3.3. Power supply control strategy.** The power supply strategy for isolated multi energy complementary building energy systems is shown in Figure 3.3. When the power generation of photovoltaic modules exceeds the sum of air source heat pumps, electric heating, and building electricity consumption (total electricity consumption), only photovoltaic modules are used for power supply; When the power generation of

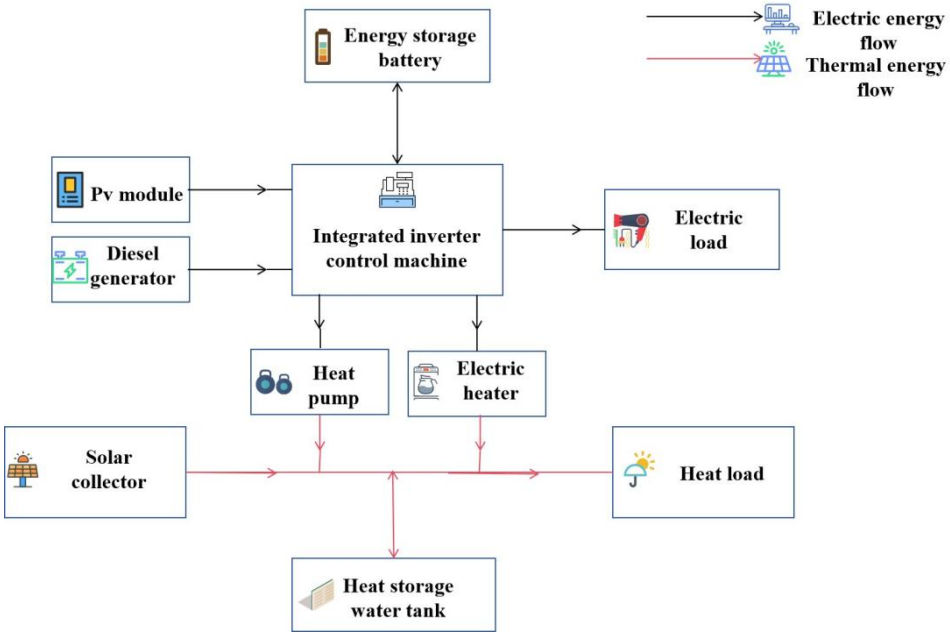


Fig. 3.1: Isolated Multi energy Complementary Building Energy System

photovoltaic modules is less than the total electricity consumption and has not yet reached the lower limit of energy storage battery discharge, priority should be given to the auxiliary photovoltaic modules powered by energy storage batteries. After reaching the lower limit of energy storage battery capacity, diesel generators should be started for power supply [15].

### 3.4. Establishment of mathematical models for equipment.

**3.4.1. Solar collectors.** The author utilizes flat plate solar collectors as the primary heating equipment. The heat collection capacity of a solar collector depends on the solar irradiance and the effective area of the collector [16]. In a stable state, ignoring the heat absorbed by the heat absorbing plate itself, the formula for calculating the solar heat collection is:

$$Q_{cu} = A_{co} \cdot [F_R \cdot (\tau\alpha)_e \cdot G - F_R \cdot U_L \cdot (T_{ci} - T_{en})] \tag{3.1}$$

In the above equation: Aco is the effective area of the solar collector, $m^2$; $T_{ci}$ is the inlet temperature of the solar collector, $^\circ C$; Ten ambient temperature, $^\circ C$.

The heat collection of a solar collector can also be expressed by the inlet and outlet temperature of the solar collector, and the calculation formula is:

$$Q_{cu} = 3600 \cdot c \cdot m_{co} \cdot (T_{co} - T_{ci}) \tag{3.2}$$

In the above formula: $T_{co}$ solar collector outlet temperature, $^\circ C$; $T_{ci}$ is the inlet temperature of the solar collector, $^\circ C$.

**3.4.2. Heat storage water tank.** The author employs the 'node method' to model the thermal stratification phenomenon in the water tank. The control functions for the solar collector side and the load side are as follows:

$$F_i^c = \begin{cases} 1, i = 1, T_{co} > T_i \\ 1, T_{i-1} \geqslant T_{co} > T_i \\ 0, i = 0 || i = N + 1 \\ 0, other \end{cases} \tag{3.3}$$

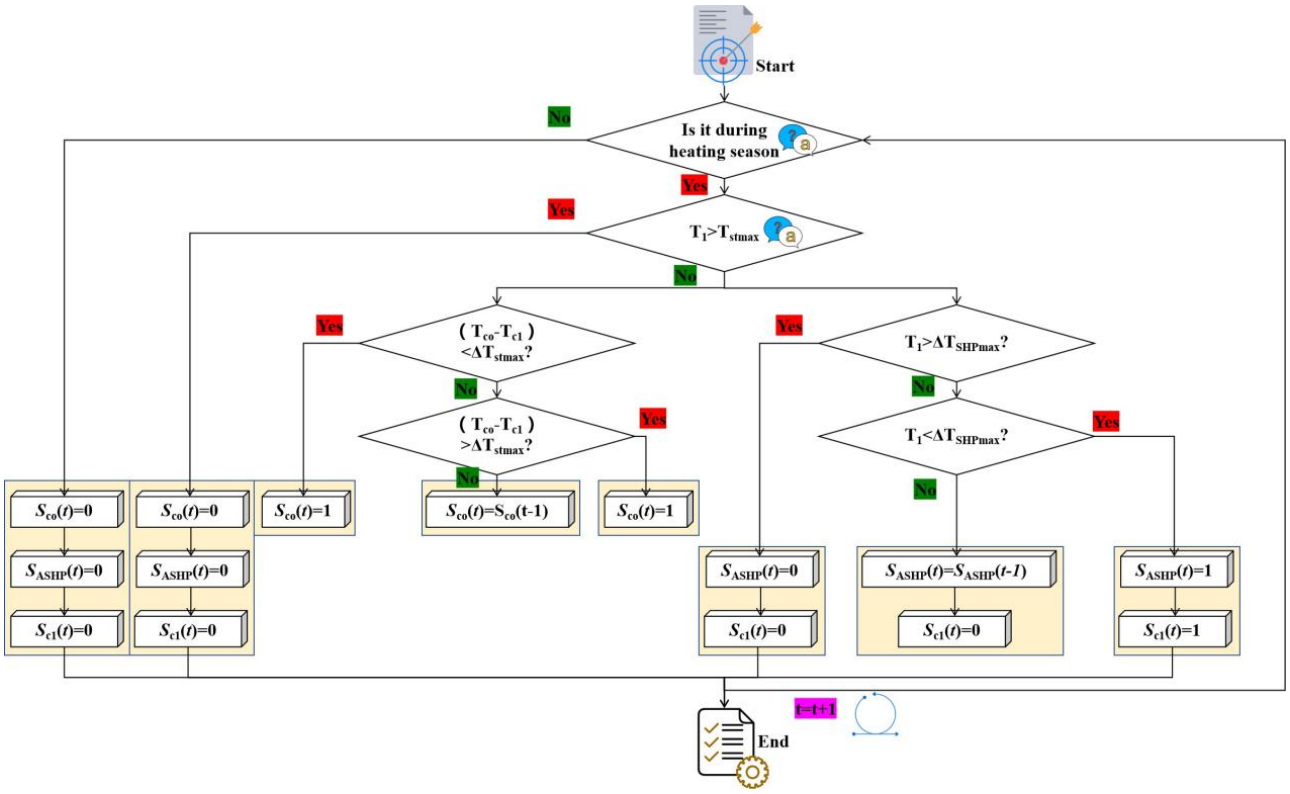


Fig. 3.2: Heating System Control Strategy

$$F_i^L = \begin{cases} 1, i = N, T_L < T_N \\ 1, T_{i-1} \geqslant T_L > T_i \\ 0, i = 0 || i = N+1 \\ 0, other \end{cases} \tag{3.4}$$

In the above equation: $T_i$ represents the average water temperature at node i of the thermal storage tank, $°C$. $T_L$ is the return water temperature on the load side, $°C$; $T_N$ is the average water temperature (lowest layer) of node N in the thermal storage tank, $°C$.

The energy balance relationship of node i is as follows:

$$\begin{aligned} m_i \cdot \frac{dT_i}{dt} = [\frac{UA}{c_p} \cdot (T_{en} - T_i) + F_i^c \cdot m_{co} \cdot (T_{co} - T_i) + \\ F_i^L \cdot m_L \cdot (T_L - T_i) + \begin{cases} \dot{m}_i \cdot (T_{i-1} - T_i), \dot{m}_i > 0 \\ \dot{m_{i+1}}(T_i - T_{i+1}), \dot{m_{i+1}} < 0 \end{cases} ] \end{aligned} \tag{3.5}$$

**3.4.3. Air source heat pump.** The author used a fitted coefficient of performance (COP) curve to calculate the heating capacity of an air source heat pump, taking into account the defrosting correction of the air source heat pump in the study. The calculation formula is:

$$COP = -0.0004 \cdot T_{en}^2 + 0.0903 \cdot T_{en} + 3.0924 \tag{3.6}$$

$$Q_{ASHP} = S_{ASHP} \cdot P_{ASHP} \cdot COP \cdot (1 - k) \tag{3.7}$$

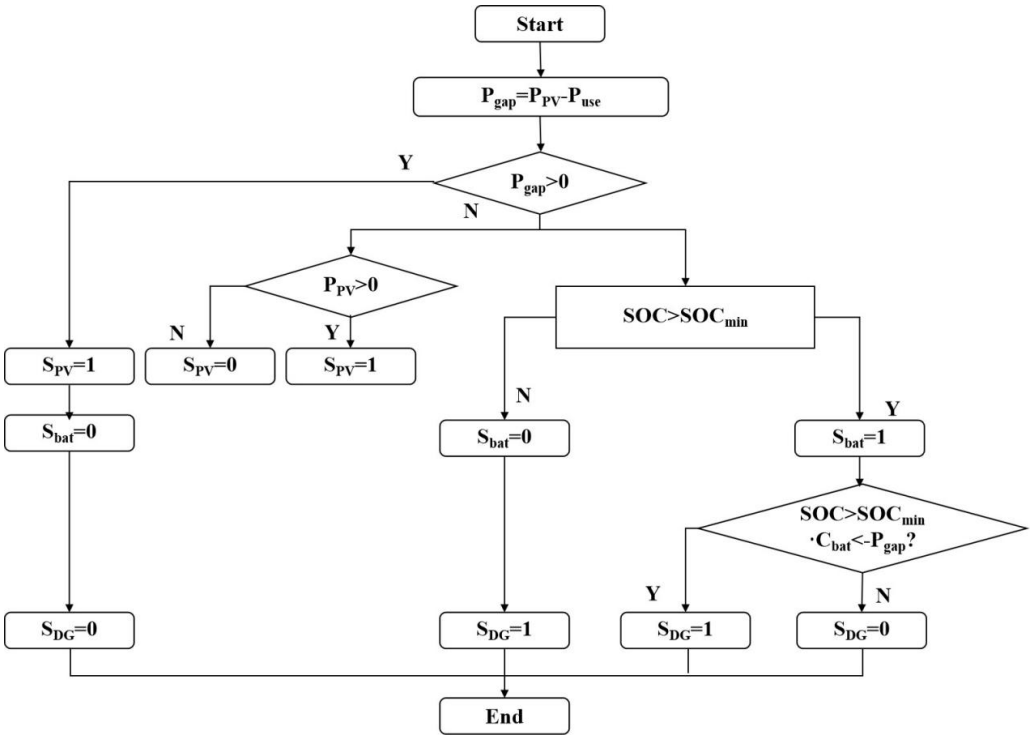


Fig. 3.3: Power Supply System Control Strategy

**3.4.4. Photovoltaic modules.** The formula for calculating the power generation of photovoltaic modules is:

$$P_{PV} = PMP_{ref} \cdot \frac{G}{1000} \cdot [1 + \gamma_{PV} \cdot (T_{cell} - 25)] \tag{3.8}$$

The above equation: $\gamma_{PV}$ is the temperature coefficient of the photovoltaic module's power generation efficiency, ranging from 0.4% to 0.6%/$°C$; $T_{cell}$ is the battery temperature, $°C$.

The battery temperature $T_{cell}$ can be calculated by equation 3.9:

$$T_{cell} = T_{en} + \frac{NOCT - 20}{800} \cdot G \tag{3.9}$$

**3.4.5. Energy storage batteries.** The State of Charge (SOC) calculation during the charging and discharging process of energy storage batteries is as follows:

$$SOC(t) = SOC(t - \Delta t) + \frac{P_{ban} \cdot \eta_{cha} \cdot \Delta t}{C_{bat}} \tag{3.10}$$

$$SOC(t) = SOC(t - \Delta t) + \frac{P_{baT} \cdot \Delta t}{\eta_{dis} \cdot C_{bat}} \tag{3.11}$$

The above equation: SOC(t) t represents the charging and discharging status of the energy storage battery at time t; $\eta_{cha}$ is the charging efficiency of the energy storage battery, taken as 1; $\eta_{dis}$ is the discharge efficiency of the energy storage battery, taken as 0.8.

**3.4.6. Diesel generator.** As an emergency power supply, the fuel consumption of diesel generators depends on their rated power and output power. The approximate mathematical expression is:

$$F_{cons} = \alpha_{DC} \cdot P_{DG} + \beta_{DG} \cdot P_{o-DG} \tag{3.12}$$

The above equation: $\alpha_{DC}$ is the coefficient of diesel generator, taken as 0.081451/kWh; $\beta_{DG}$ is the coefficient of diesel generator, taken as 0.2461/kWh.

**3.5. Electric load model.** The author divides the user side electricity load into three categories: 1) Basic electricity load: closely related to the living habits of residents, and cannot change their energy consumption mode and time; 2) Translatable electrical load: The power supply time of the load can be changed, but the load needs to be moved as a whole and cannot be interrupted [17]. 3) Transferable electricity load: The electricity consumption during each time period can be flexibly adjusted, but it must ensure that the total load of the entire cycle remains unchanged after the transfer compared to before the transfer. The specific modeling of various flexible electrical loads is detailed in the following text [18].

**3.5.1. Translatable electrical load.** Assuming a unit scheduling time of 1 hour, for the translatable electrical load Lmove, the power distribution before participating in scheduling is expressed as:

$$L^*_{move} = [0, \cdots, P_{more}(t_s), P_{more}(t_s+1), \cdots, P_{move}(t_s+t_b), \cdots, 0] \tag{3.13}$$

Assuming the translatable interval is $[t_{move}, t_{move}]$, use the 0-1 variable a to represent the translational state of $L_{move}$ at a certain time period t. When a=1, it indicates that Lmove starts translational from time t; when a=0, it indicates that $L_{move}$ does not translational. The set of starting time periods $S_{move}$ is:

$$S_{move} = [t_{move-}, t_{move} - t_D + 1] \tag{3.14}$$

If $t \in [t_{mox}, t_{moxot} - t_D + 1]$ and $t \neq t_s$, then the power distribution of $L^*_{max}$ shifting from time t $\epsilon$ to $L_{max}$ at time t is:

$$L_{move} = [0, \cdots, P_{move}(t), P_{move}(t+1), \cdots, P_{mover}(t+t_D), \cdots, 0] \tag{3.15}$$

**3.5.2. Transferable electrical load.** Assuming that the transferable interval of the transferable electrical load $L_{trm}$ is $[t_{tan}, t_{trmn}]$, the 0-1 variable b represents the transfer state of $L_{trom}$ at time t, and b(t)=1 represents the transfer of power $P_{tan}$ in $L_{trn}$ at time t. The power constraints after the transfer are as follows:

$$b(t) \cdot P^{tran}_{min} \leqslant P_{tran}(t) \leqslant b(t) \cdot P^{tran}_{max} \tag{3.16}$$

If there are no restrictions on the load transfer period, there may be a phenomenon of load transfer to multiple single periods, which is manifested externally as frequent equipment startup and shutdown. Therefore, it is necessary to limit the minimum duration of load transfer operation:

$$\sum_{\tau=t}^{+T^{tman}_{mimen}-1} b(\tau) \geqslant T^{tran}_{min} \cdot (b(\tau) - b(\tau-1)) \tag{3.17}$$

By using the above model, the adjusted flexible electrical load can be obtained, and the total electrical load can be calculated as follows:

$$P_{active} = P_{move} + P_{tran} \tag{3.18}$$

$$P_{load} = P_{base} + P_{acctive} \tag{3.19}$$

**3.6. Heat load model.**

**3.6.1. Calculation of building heat load.** The heat load calculation model for the room is:

$$Q_{load} = q_V \cdot V \cdot (T_{in} - T_{en}) \tag{3.20}$$

**3.6.2. Heat load model considering flexible loads.** Assuming that the indoor temperature varies between and the variable di represents the difference between the upper limit of the indoor temperature and the actual indoor temperature, the indoor temperature is:

$$T_{in}(t) = T_{inmax} - d_i(t) \tag{3.21}$$

By substituting formula 3.21 into formula 3.20, a heat load model considering flexible loads can be obtained [19].

**3.7. Optimization Model.**

**3.7.1. Objective function.** The author sets the annual cost of isolated multi-energy complementary building energy systems as the objective function for optimization. The annual cost of the system comprises two components: the annualized investment value and the operation and maintenance costs. The mathematical expression is:

$$min(F) = min(C_1 + C_{om}) \tag{3.22}$$

The mathematical expression for the annual value C1 of system investment is:

$$C_1 = \left[ P_h \cdot \frac{i_{ATT}}{1 - (1 + i_AIT) - T_h} + P_e \cdot \frac{i_{ATT}}{1 - (1 + i_{AIT} - T_c)} + C_{bat} \cdot \frac{i_{AIT}}{1 - (1 + i_{AIT}) - T_{Lac}} \right] \tag{3.23}$$

$$P_h = C_{1\_co} \cdot A_{co} + C_{1ASHP} \cdot P_{ASHP} + C_{1\_st} \cdot V_{st} \tag{3.24}$$

$$P_e = C_{1\_PV} \cdot PMP_{ref} + C_{1\_DG} \cdot P_{DG} + C_{1\_acc} \tag{3.25}$$

$$C_{bat} = C_{1Lhat} \cdot C_{bat} \tag{3.26}$$

The operating cost of the system is the fuel cost generated by diesel power generation, and the mathematical expression for operating and maintenance costs is:

$$C_{om} = C_F \cdot F_{cons} + C_1 \cdot \zeta \tag{3.27}$$

**3.7.2. Constraints.** The capacity and operation of each device in the system should be within a certain reasonable range, and the corresponding equipment capacity and power range are:

$$0 \leqslant A_{co} \leqslant A_{co,max} \tag{3.28}$$

$$0 \leqslant V_{st} \leqslant V_{st,max} \tag{3.29}$$

$$0 \leqslant PMP_{ref} \leqslant PMP_{ref,max} \tag{3.30}$$

$$0 \leqslant C_{hat} \leqslant C_{hat,max} \tag{3.31}$$

$$0 \leqslant P_{o-DG} \leqslant P_{DG} \tag{3.32}$$

$$0 \leqslant P_{ASHP} \leqslant \frac{Q_{load,max}}{COP} \tag{3.33}$$

$$SOC_{min} \leqslant SOC \leqslant SOC_{max} \tag{3.34}$$

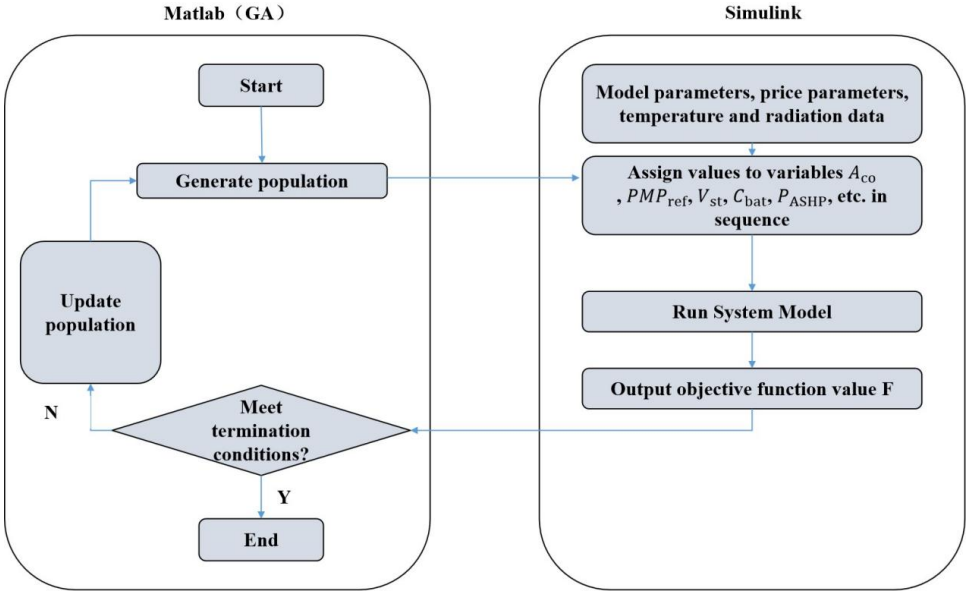


Fig. 3.4: System Optimization Flowchart

Table 3.1: Unit Costs of System Equipment

| parameter | numerical value | parameter | numerical value |
|---|---|---|---|
| $C_{I\_co}/(yuan \cdot m^{-2})$ | 800 | $C_{I\_ASHP}/(yuan \cdot KWW^{-1})$ | 2000 |
| $C_{I\leqslant 1}/(yuan \cdot m^{-3})$ | 500 | $C_{I\_PV}/(yuan \cdot KWW^{-1})$ | 8000 |
| $C_{.1bat}/(yuan \cdot kWh^{-1})$ | 800 | $C_{I\_DG}/(yuan \cdot KWW^{-1})$ | 1500 |

**3.7.3. Optimization methods.** The author established a system model using Simulink, and based on genetic algorithm, jointly solved it using Simulink and Matlab optimization toolbox. The optimization process is shown in Figure 3.4. At the beginning of the iteration, the decision variables are passed to the Simulink module, and the objective function value is calculated using dynamic simulation of the system and returned to MATLAB for judgment [20]. If the termination condition is satisfied, the iteration stops and the optimal result is achieved; otherwise, the iteration continues until the termination condition is met.

**3.8. Input parameter settings.** The author studied calculating a time step of 1 hour, setting different population sizes and maximum iterations for different scenarios, with a maximum population size of 1490 and a maximum iteration of 400. The unit costs of each equipment involved in the calculation process are shown in Table 3.1.

**3.9. Experimental Analysis.** The author takes a rural residential building as the research object, with a heating area of 68m2 and an indoor calculated temperature of 18 $^{\circ}C$.

The daily electrical load of buildings includes basic electrical load, translatable electrical load 1, translatable electrical load 2, and transferable electrical load. The parameters of each flexible load are shown in Table 3.2. The author's research assumes that the hourly electricity consumption of the building is the same during winter, transition season, and typical summer days.

The author studied using annual cost values as performance evaluation indicators for isolated multi energy complementary building energy systems, with carbon dioxide emissions as auxiliary performance evaluation

Table 3.2: Flexible Load Parameters

| Types | Translatable electrical load | | | | | | | | |
|---|---|---|---|---|---|---|---|---|---|
| | $t_s$ | $t_D/h$ | $t_{mone} \sim t_{monet}$ | $t_s$ | $t_D/h$ | $t_{mone} \sim t_{monet}$ | $t_s$ | $t_D/h$ | $t_{mone} \sim t_{monet}$ |
| 1 | 19:00 | | | 3 | | | 08:00-20:00 | | |
| 2 | 11:00 | | | 2 | | | 08:00-20:00 | | |
| Transferable electrical load | $T_{min}^{tam}/h$ | | | $P_{min} \sim P_{man}/kW$ | | | $t_{tran} \sim t_{tran}$ | | |
| | 2 | | | $0.15 \sim 0.25$ | | | $08:00-20:00$ | | |

Table 4.1: Optimization Results of Multi energy Complementary Building Energy System Design

| Parameter | Scenario 1 | Scenario 2 | Scenario 3 | Scenario 4 |
|---|---|---|---|---|
| $A_{co}/m^2$ | 16.17 | 11.72 | 9.70 | 9.45 |
| $P_{ssH}/kW$ | 2.60 | 2.07 | 1.31 | 2.06 |
| $V_s/m^3$ | 9.84 | 9.87 | 7.88 | 8.47 |
| $PMP/kW$ | 2.03 | 2.00 | 1.88 | 1.81 |
| $C_{ba}/kWh$ | 68.87 | 71.26 | 66.60 | 64.43 |
| $P_{Dc}/kW$ | 0.05 | 0 | 0.04 | 0 |
| F/ ten thousand yuan | 2.63 | 2.50 | 1.72 | 1.66 |
| $E_{Co_2}/kg$ | 120.35 | 0 | 92.13 | 0 |
| Cost savings rate/% | - | 5.13 | 33.00 | 35.40 |

indicators. The formula for calculating the annual carbon dioxide emissions of diesel generators is:

$$E_{CO_2} = \sum_{t=1}^{8760} F_{cons}(t) \cdot EF \tag{3.35}$$

**4. Results and Discussion.** To analyze the impact of flexible loads on the performance of multi-energy complementary building energy systems, the author establishes four scenarios for comparative analysis: Scenario 1, which does not consider flexible load regulation; Scenario 2, which considers flexible electrical load regulation; Scenario 3, which considers flexible heat load regulation; and Scenario 4, which considers both flexible electrical and thermal load regulation. The optimization results for the multi-energy complementary building energy system under these four scenarios are presented in Table 4.1.

From Table 4.1, it can be seen that in Scenario 1, the solar collector, air source heat pump, and diesel generator have the highest capacity. In scenario 2, the equipment capacity of the solar collector and air source heat pump has decreased compared to scenario 1, but the capacity of photovoltaic modules and energy storage batteries is the highest among all scenarios. Compared with scenario 1, the annual carbon dioxide emissions have decreased by 120.35kg, and the annual system cost has decreased by 5.13%. Compared with Scenario 1 and Scenario 2, the capacity of equipment such as solar collectors, air source heat pumps, and photovoltaic modules in Scenario 3 has all decreased. Compared with Scenario 1, the annual carbon dioxide emissions have decreased by 28.11kg, and the annual system cost has decreased by 33.01%. In scenario 4, the area of the solar collector, the capacity of photovoltaic modules and energy storage batteries are the lowest among all scenarios. Compared with scenario 1, the annual carbon dioxide emissions are reduced by 120.35kg, and the annual system cost is reduced by 35.4%, resulting in the best regulation effect.

Upon integrating flexible electrical loads into regulation, the load schedule aligns with peak photovoltaic output periods, effectively utilizing solar power and thereby reducing the required capacities of energy storage batteries and diesel generators. When both flexible thermal and electrical loads are regulated concurrently, the capacities needed for photovoltaic modules, energy storage batteries, and diesel generators reach their minimum across all scenarios; After the participation of flexible heat load regulation, the indoor temperature decreases and the fluctuation amplitude is large. When flexible electricity and heat loads are simultaneously regulated, indoor temperature fluctuations tend to flatten.

**5. Conclusion.** The author proposes the use of digital twins and genetic algorithms for the study of building energy systems. The author analyzes the impact of flexible loads on the optimization design of multi energy complementary building energy systems and establishes a multi energy complementary building energy system optimization model and flexible load model in MATLAB/Simulk, mainly consisting of photovoltaic modules and solar collectors. The genetic algorithm is used to optimize the capacity of various equipment in the system, and the following conclusions are obtained:) Compared with not considering flexible loads, when flexible electricity loads, flexible heat loads, and flexible electricity/heat loads participate in regulation, the annual cost of the system is reduced by 5.24%, 33.11%, and 35.5%, respectively, and the annual carbon dioxide emissions are reduced by 120.46, 28.22, and 120.46kg, respectively. When flexible thermal and electrical loads are simultaneously regulated, the best reduction effect is achieved for the annual value of system costs and annual carbon dioxide emissions; After the participation of flexible electrical loads in regulation, the load shifts towards the photovoltaic output period, timely consuming photovoltaic power generation and reducing the capacity of energy storage batteries and diesel generators. When flexible thermal and electrical loads are simultaneously regulated, the capacity of photovoltaic modules, energy storage batteries, and diesel generators is the lowest value among all scenarios; After the participation of flexible heat load regulation, the indoor temperature decreases and the fluctuation amplitude is large. When flexible electricity and heat loads are simultaneously regulated, indoor temperature fluctuations tend to flatten.

REFERENCES

[1] Zhang, J. (2023). The effect of carbon tax incidence on household energy demand and welfare in the u.s. Environmental Science and Pollution Research, 30(5), 13210-13223.
[2] Li, M., Zhu, K., & Lu, Q. Y. K. (2023). Technical and economic analysis of multi-energy complementary systems for net-zero energy consumption combining wind, solar, hydrogen, geothermal, and storage energy. Energy conversion & management, 295(11), 1-17.
[3] Abdelmoumene, A., Bentarzi, H., Iqbal, A., & Krama, A. (2024). Developments and trends in emergency lighting systems: from energy-efficiency to zero electrical power consumption. Life Cycle Reliability and Safety Engineering, 13(2), 129-145.
[4] Tanriverdi, B., & Gedik, G. Z. (2023). Importance of hvac system selection in reducing the energy consumption of building retrofits–case study: office building in london. Civil Engineering and Architecture, 11(1), 217-227.
[5] Teng, J., Yin, H., & Wang, P. (2023). Study on the operation strategies and carbon emission of heating systems in the context of building energy conservation. Energy Science And Engineering, 11(7), 2421-2430.
[6] Roodkoly, S. H., Fard, Z. Q., Tahsildoost, M., Zomorodian, Z., & Karami, M. (2024). Development of a simulation-based ann framework for predicting energy consumption metrics: a case study of an office building. Energy efficiency, 17(1), 1-24.
[7] Hawks, M. A., & Cho, S. (2024). Review and analysis of current solutions and trends for zero energy building (zeb) thermal systems. Renewable & sustainable energy reviews, 189(Jan. Pt.B), 1-15.
[8] Altes-Buch, Q., Quoilin, S., & Lemort, V. (2022). A modeling framework for the integration of electrical and thermal energy systems in greenhouses. Building Simulation, 15(5), 779-797.
[9] Bazenkov, N. I., Dushin, S. V., & Mikhail V. GoubkoVsevolod O. KorepanovYuriy M. RassadinLeonid A. SeredaAlla G. Shinkaryuk. (2022). An office building power consumption dataset for energy grid analysis and control algorithms. ifac papersonline, 55(9), 111-116.
[10] Libralato, M., D'Agaro, P., & Cortella, G. (2023). Development of an energy digital twin from a hotel supervision system using building energy modelling. IOP Publishing Ltd, 53(Oct. Pt.C), 1-8.
[11] Ohmura, T., Shimomura, Y., Egawa, R., & Takizawa, H. (2023). Toward building adigital twin ofjob scheduling andpower management onanhpc system, 7(18), 4654-4667.
[12] Hou, Y., & Volk, R. (2022). Conceptual design of a digital twin-enabled building envelope energy audits and multi-fidelity simulation framework for a computationally explainable retrofit plan. Proceedings of the 9th ACM International Conference on Systems for Energy-Efficient Buildings, Cities, and Transportation, 30(5), 1-22.
[13] Nobuyoshi, Y. J. R., Antonio, V. O. A., & Angelo Peixoto da Costa J.Suemy Arruda Michima P.de Novaes Pires Leite G.Claudius Nunes Silva H.Gabriel Carvalho de Oliveira E.Tiba C. (2023). Real-time energy and economic performance of the multi-zone photovoltaic-drive air conditioning system for an office building in a tropical climate. Energy conversion & management, 297(Dec.), 1-21.
[14] Cheraghi, R., & Hossein, J. M. (2023). Multi-objective optimization of a hybrid renewable energy system supplying a residential building using nsga-ii and mopso algorithms. Energy conversion & management, 294(Oct.), 1-20.
[15] Juan M. González-Caballín Sánchez, A. Meana-Fernández, J.C. Ríos-Fernández, & A.J. Gutiérrez Trashorras. (2023). Characterization of housing stock for energy retrofitting purposes in spain. Building Simulation, 16(6), 947-962.
[16] Saleh BabaaAbdul Aziz Al RawahiAngala SubramanianAbdullah Humaid AlshibliShahid KhanMartin KhzouzMuneer Ahmed-Ibrahim Ashrafi. (2022). Smart building design to improve the energy consumption at an office room, 13(9), 209-221.
[17] Wang, H., Ma, W., & Wang, Z. L. C. (2022). Multiscale convolutional recurrent neural network for residential building electricity consumption prediction. Journal of Intelligent & Fuzzy Systems: Applications in Engineering and Technology, 43(3), 3479-3491.

[18] Tahmasebi, M., & Nassif, N. (2022). An intelligent approach to develop, assess and optimize energy consumption models for air-cooled chillers using machine learning algorithms. American journal of engineering and applied sciences, 15(3), 220-229.
[19] Gholamian, E., Bagheri, B. R., & Zare, V. R. S. F. (2022). The effect of incorporating phase change materials in building envelope on reducing the cost and size of the integrated hybrid-solar energy system: an application of 3e dynamic simulation with reliability consideration. Sustainable Energy Technologies and Assessments, 52(Aug. Pt.B), 1-13.
[20] Aliabadi, A. A., Chen, X., & Yang, A. S. K. (2023). Retrofit optimization of building systems for future climates using an urban physics model. Building and environment, 243(Sep.), 1-20.

*Edited by:* Hailong Li
*Special issue on:* Deep Learning in Healthcare
*Received:* Jun 24, 2024
*Accepted:* Aug 12, 2024